represented with (Fig. 6A) and without (Fig. 6B) the adjacent heart can be compared and reveal the anatomic relationship between the two organs. Indeed, the recess formed by the left ventricle is a characteristic temporal feature of the cranial surface of the liver between CS17 and CS19.

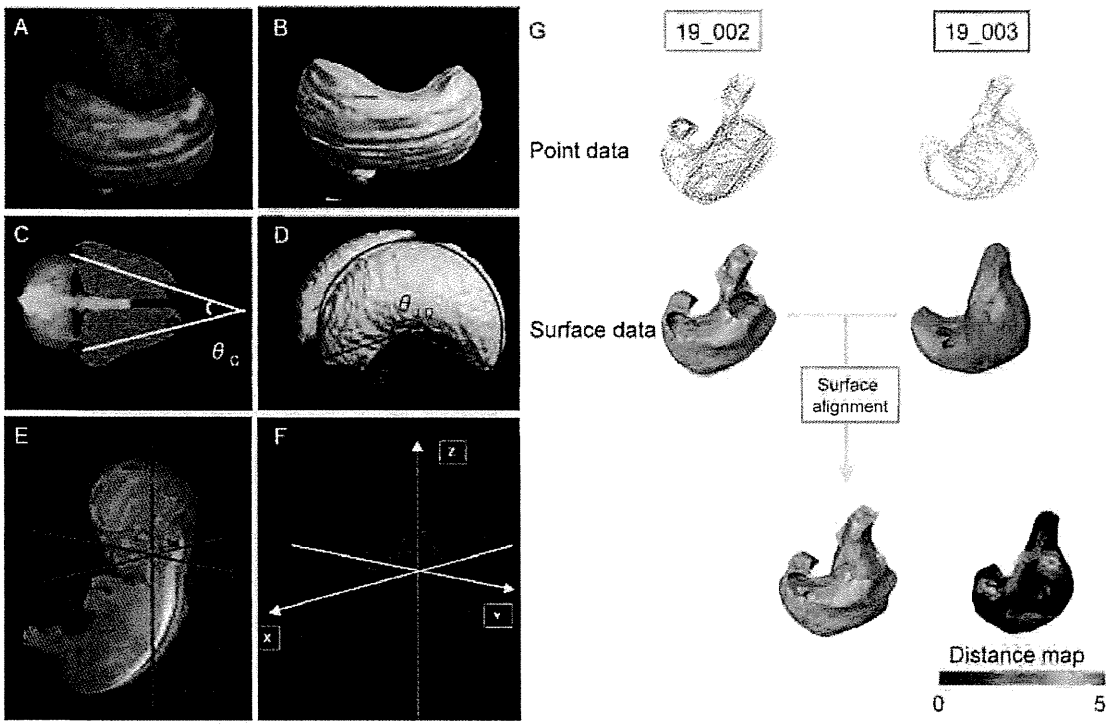

Fig. 6. Analytical methods on 3D reconstructed images.
A,B) Three-dimensional reconstructed image of the embryonic liver (CS18) with (A) and without (B) the heart demonstrate the anatomical relationship between the two organs.
C-D) Morphometry from 3D images of lateral cerebral ventricles (CS22): C) Cranial view. The blue shaded areas represent the lateral ventricles and the angle formed by the bilateral ventricles was measured. D) Lateral view. The viewing perspective was modified allowing measurement of radius and central angles.
E,F) Three-dimensional coordinates of anatomical landmarks are useful for monitoring movements between developmental stages and characterize relationships between anatomical landmarks.
G) Surface alignment provides an averaged view of the organ of interest. Here, the stomachs from two embryos at CS19 were aligned.

3.4.2 Morphometry

Three-dimensional images can be exploited to measure morphological changes in a quantitative manner. Using the image data, not only the total volumes, but also the lengths, angles and areas of the regions and organs of interest can be measured accurately (Fig. 6C, 6D). Morphometric data are useful for evaluating and characterizing developmental features of the embryo, and also for screening for abnormalities.

3.4.3 Three-dimensional coordinates

MRI data sets are provided as cuboid of 256x 256x512 voxels and thus allows for three-dimensional coordinates to be assigned to embryonic landmarks (Fig. 6E, 6F). Three-dimensional coordinates of anatomical landmarks are useful for monitoring the movements of landmarks and define their anatomical relationships during prenatal development.

3.4.4 Surface alignment

Multiple images can be aligned resulting in averaged images and compatibility rates are indicated by color gradients. An embryonic stomach was segmented from 2D sequential images (Fig. 6G) and surface data originating from point datasets of each respective embryo were processed.

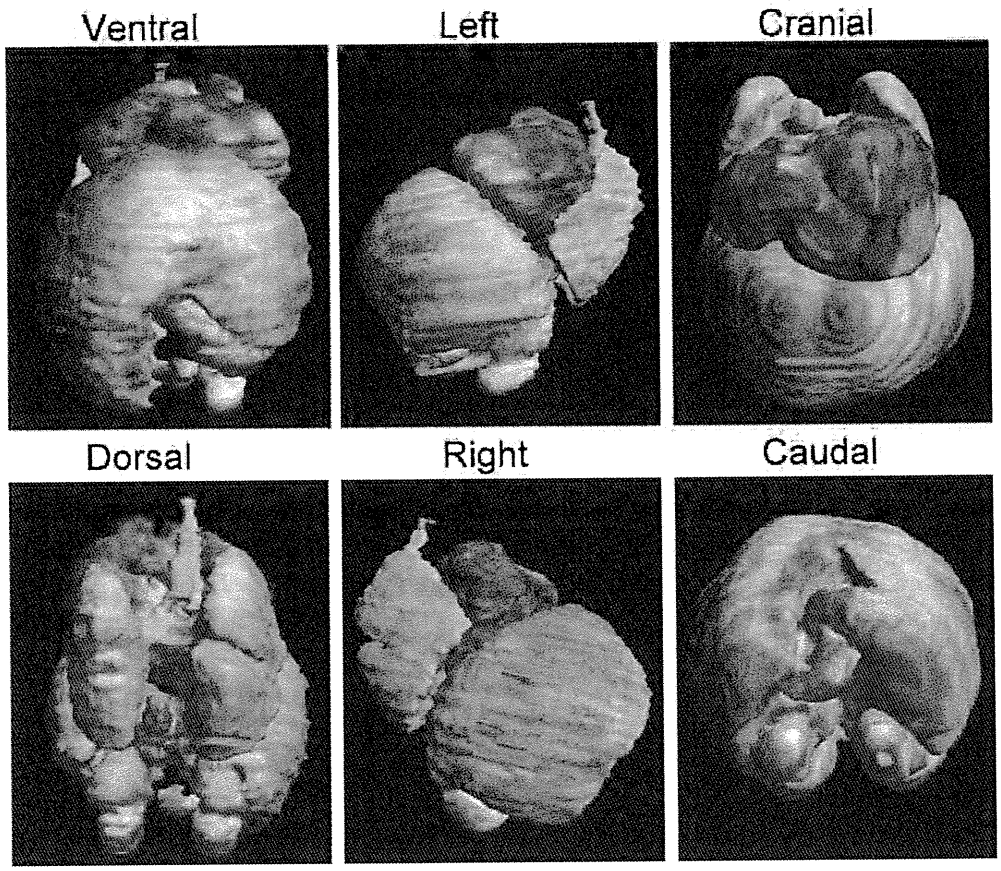

Fig. 7. Representative 3D images of the embryonic liver at CS22 with adjacent organs. Liver (green), lung (blue), heart (red), stomach (brown), kidney (yellow), and adrenal glands (purple) were segmented from 2D sequential images and reconstructed in 3D.

3.5 Representative 3D images of the embryo and fetus organs

Three-dimensional images of various organs in the embryo or the fetus were constructed and representative images of embryonic liver and cerebral ventricles are shown in Fig. 7 and Fig. 8, respectively.

4. Perspective

Recent advances in imaging techniques allow for anatomical analyses of human embryo specimens in earlier stages and for clinical prenatal diagnosis during the first trimester. Current information on normal development during embryonic stages, however, remains insufficient to achieve such clinical evaluation. Further investigations are critical to gain insight into the dynamic and complex events occurring during organogenesis. Dynamic modeling of embryonic structures and 3D digital reconstructions will be valuable tools to elucidate the complex anatomical changes taking place during early embryonic stages. They will serve as useful references to evaluate the appropriate development of embryonic organs, and understand how adjacent organs affect each other's morphology. Now and in the future, this type of information will be indispensable to researchers and to clinicians, and more particularly in respect to the obstetrical ultrasonography conducted in the early gestational weeks.

5. Appendix (softwares)

The use of software is necessary for reconstruction into 3D images and morphometric analysis. The software programs used in this chapter are summarized below. More information is available on the URL of their respective websites.

5.1 OsiriX (http://www.osirix-viewer.com/index.html)

OsiriX is an image processing software dedicated to DICOM images produced by imaging equipment (e.g. MRI, CT, PET, PET-CT, SPECT-CT, Ultrasounds). It is fully compliant with the DICOM standard for image communication and image file formats. OsiriX is able to receive images transferred by DICOM communication protocol from any PACS or imaging modality.

5.2 Image J (http://rsbweb.nih.gov/ij/index.html)

ImageJ is a public domain Java image-processing program inspired from the NIH Image software developed for Macintosh. It runs, either as an online applet or as a downloadable application, on any computer with a Java 1.4 or later virtual machine.

5.3 Delta viewer (http://delta.math.sci.osaka-u.ac.jp/DeltaViewer/index.html)

DeltaViewer is an application program developed for Apple Macintosh. DeltaViewer reads sequences of cross-sectional images of a sample in a manner similar to confocal laser microscopes, CT, MRI, optical or electron microscopes. The computer program then reconstructs the surface of the scanned sample, and displays the image on the screen. The image can then be freely rotated, for characterization of 3D shapes and spatial relationships.

5.4 Avizo (http://www.vsg3d.com/avizo/overview)

Avizo® software is a powerful, multifaceted tool for visualizing, manipulating, and understanding scientific and industrial data. Wherever 3D data sets need to be processed, in materials science, geosciences, environmental or engineering applications, Avizo offers abundant state-of-the-art features within an intuitive workflow and easy-to-use graphical user interfaces.

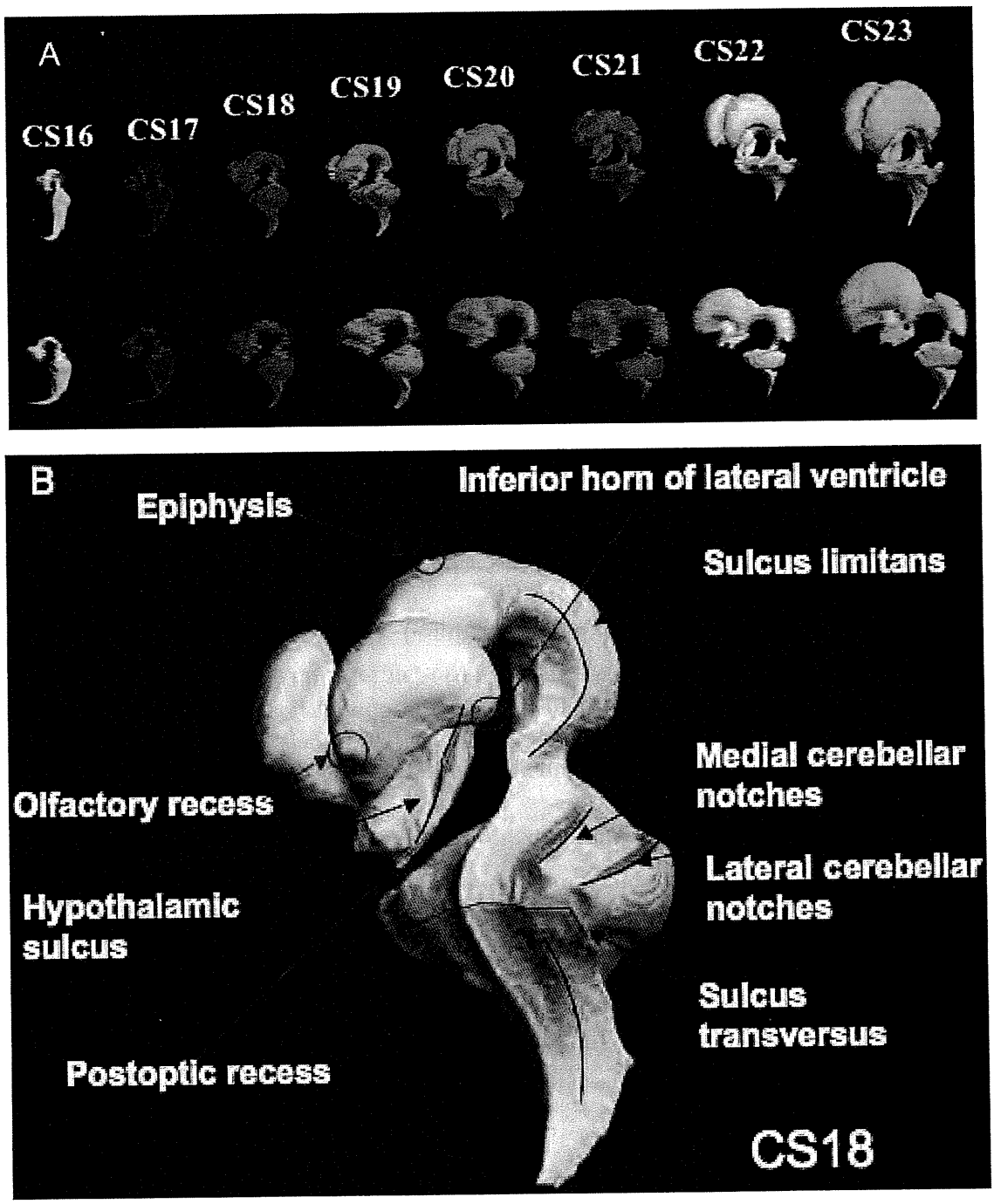

Fig. 8. (A) Representative 3D images of cerebral ventricles between Carnegie stage 16 and stage 23. (B) 3D image illustrating the conservation of anatomic landmarks.

5.5 FMRIB Software Library (FSL) (http://www.fmrib.ox.ac.uk/fsl/index.html)

FSL is a comprehensive library of analytical tools for fMRI (functional magnetic resonance imaging), MRI and DTI (Diffusion tensor imaging) brain imaging data. FSL was mainly

developed by members of the Analysis Group at the FMRIB, Oxford, UK. FSL runs on Apple and PCs (Linux and Windows), and is easy to install. Most of the tools can be run either from the command line or as "point-and-click" graphical user interfaces.

5.6 Analyze (http://www.mayo.edu/bir/Software/Analyze/Analyze.html)

Analyze 10.0 is a powerful, comprehensive software package for multi-dimensional display, processing, and measurement of multi-modality biomedical images. Product of more than 25 years of biomedical imaging research and development at Mayo Clinic, this integrated, total solution allows you to significantly enhance your multidimensional biomedical imaging productivity.

6. Acknowledgments

We would like to thank Ms Merumo Ueda, Ms Nami Uematsu, Ms Kyoko Nakajima, and Ms Sayuri Nunomura at the Kyoto University Graduate School of Medicine, Human Health Science, for conducting some of the experiments; Ms Chigako Uwabe at the Congenital Anomaly Research Center for technical assistance in handling human embryos; Prof. Masaaki Wada at the Graduate School of Information Science and Technology at Osaka University for help on the use of the DeltaViewer software; Prof. Katsumi Kose and Dr. Yoshimasa Matsuda at the Institute of Applied Physics at University of Tsukuba and Dr. Stasia A Anderson at the NHLBI Animal MRI Core, National Institutes of Health, for technical help with MR imaging; and Prof. Kohei Shiota, Vice President of Kyoto University, for his support and guidance on the project. The researches were financially supported by Grants #228073, #238058, #21790810 and #22591199 from the Japan Society for the Promotion of Science (JSPS) and the Japan Science and Technology (JST) institute for Bioinformatics Research and Development (BIRD). The researches were also supported by Japan Spina Bifida and Hydrocephalus Research Foundation, and Konica Minolta Science and Technology Foundation. The studies presented in this chapter were approved by the Medical Ethics Committee at Kyoto University Graduate School of Medicine (Kyoto, Japan).

7. References

Becker, B. P. & Bonse, U. 1974. The skew-symmetric two-crystal X-ray interferometer. *Journal of Applied Crystallography,* 7, 593-598.

Bone, S. N., Johnson, G. A. & Thompson, M. B. 1986. Three-dimensional magnetic resonance microscopy of the developing chick embryo. *Invest Radiol,* 21, 782-7.

Born, G. 1883. Die Plattenmodelliermethode. *Archiv für mikroskopische Anatomie.* 22, 584-99.

Effmann, E. L., Johnson, G. A., Smith, B. R., Talbott, G. A. & Cofer, G. 1988. Magnetic resonance microscopy of chick embryos in ovo. *Teratology,* 38, 59-65.

Haishi, T., Uematsu, T., Matsuda, Y. & Kose, K. 2001. Development of a 1.0 T MR microscope using a Nd-Fe-B permanent magnet. *Magnetic resonance imaging,* 19, 875-80.

Heard, O. O. 1951. Section compression photographically rectified. *The Anatomical record,* 109, 745-55.

Heard, O. O. 1953. The influence of surface forces in microtomy. *The Anatomical record,* 117, 725-39.

Heard, O. O. 1957. Methods used by C.H. Heuser in preparing and sectioning early embryos. *Contributions to Embryology,* 36, 1-18.

Matsuda, Y., Ono, S., Otake, Y., Handa, S., Kose, K., Haishi, T., Yamada, S., Uwabe, C. & Shiota, K. 2007. Imaging of a large collection of human embryo using a super-parallel MR microscope. *Magnetic resonance in medical sciences : MRMS : an official journal of Japan Society of Magnetic Resonance.* 6, 139-46.

Matsuda, Y., Utsuzawa, S., Kurimoto, T., Haishi, T., Yamazaki, Y., Kose, K., Anno, I. & Marutani, M. 2003. Super-parallel MR microscope. *Magnetic resonance in medicine : official journal of the Society of Magnetic Resonance in Medicine / Society of Magnetic Resonance in Medicine.* 50, 183-9.

Momose, A. & Fukuda, J. 1995. Phase-contrast radiographs of nonstained rat cerebellar specimen. *Medical physics,* 22, 375-9.

Momose, A., Takeda, T., Itai, Y. & Hirano, K. 1996. Phase-contrast X-ray computed tomography for observing biological soft tissues. *Nature medicine.* 2, 473-5.

Nakashima, T., Hirose, A., Yamada, S., Uwabe, C., Kose, K. & Takakuwa, T. 2011. Morphometric analysis of the brain vesicles during the human embryonic period by magnetic resonance microscopic imaging. Congenital Anomalies. doi: 10.1111/j.1741-4520.2011.00345.x

Nishimura, H. 1975. Prenatal versus postnatal malformations based on the Japanese experience on induced abortions in the human being. . *In:* BLANDEU, R. (ed.) *Aging Gamates.* Basel: S. Karger AG.

Nishimura, H., Takano, K., Tanimura, T. & Yasuda, M. 1968. Normal and abnormal development of human embryos: first report of the analysis of 1,213 intact embryos. *Teratology,* 1, 281-90.

O'Rahilly, R. 1988. One Hundred Years of Human Embryology. *In:* KALTER, H. (ed.) *Issues and Reviews in Terratology* New York: Plenum Press.

O'Rahilly, R. & Müller, F. 1987. *Developmental stages in human embryos: including a revision of Streeter's "horizons" and a survey of the Carnegie Collection.,* Washington, DC, Carnegie Institution of Washington Publication.

Rohlf, F. J. & Bookstein, F. L. 1990. *Proceedings Of The Michigan Morphometrics Workshop,* Ann Arbor, MI, University of Michigan Museum of Zoology.

Rosenthal, J., Mangal, V., Walker, D., Bennett, M., Mohun, T. J. & Lo, C. W. 2004. Rapid high resolution three dimensional reconstruction of embryos with episcopic fluorescence image capture. *Birth defects research. Part C, Embryo today : reviews,* 72, 213-23.

Shiota, K. 1991. Development and intrauterine fate of normal and abnormal human conceptuses. *Congenital Anomalies,* 31, 67-80.

Shiota, K., Yamada, S., Nakatsu-Komatsu, T., Uwabe, C., Kose, K., Matsuda, Y., Haishi, T., Mizuta, S. & Matsuda, T. 2007. Visualization of human prenatal development by magnetic resonance imaging (MRI). *American journal of medical genetics. Part A,* 143A, 3121-6.

Smith, B. R. 1999. Visualizing human embryos. *Scientific American,* 280, 76-81.

Smith, B. R. 2000. Magnetic resonance imaging analysis of embryos. *Methods in molecular biology,* 135, 211-6.

Smith, B. R. 2001. Magnetic resonance microscopy in cardiac development. *Microscopy research and technique,* 52, 323-30.

Smith, B. R., Effmann, E. L. & Johnson, G. A. 1992. MR microscopy of chick embryo vasculature. *Journal of magnetic resonance imaging: JMRI.* 2, 237-40.

Smith, B. R., Huff, D. S. & Johnson, G. A. 1999. Magnetic resonance imaging of embryos: an Internet resource for the study of embryonic development. *Computerized medical imaging and graphics : the official journal of the Computerized Medical Imaging Society,* 23, 33-40.

Smith, B. R., Johnson, G. A., Groman, E. V. & Linney, E. 1994. Magnetic resonance microscopy of mouse embryos. *Proc Natl Acad Sci U S A,* 91, 3530-3.

Smith, B. R., Linney, E., Huff, D. S. & Johnson, G. A. 1996. Magnetic resonance microscopy of embryos. *Computerized medical imaging and graphics: the official journal of the Computerized Medical Imaging Society.* 20, 483-90.

Weninger, W. J., Geyer, S. H., Mohun, T. J., Rasskin-Gutman, D., Matsui, T., Ribeiro, I., Costa Lda, F., Izpisua-Belmonte, J. C. & Muller, G. B. 2006. High-resolution episcopic microscopy: a rapid technique for high detailed 3D analysis of gene activity in the context of tissue architecture and morphology. *Anatomy and embryology,* 211, 213-21.

Weninger, W. J. & Mohun, T. 2002. Phenotyping transgenic embryos: a rapid 3-D screening method based on episcopic fluorescence image capturing. *Nature genetics,* 30, 59-65.

Yamada, S., Itoh, H., Uwabe, C., Fujihara, S., Nishibori, C., Wada, M., Fujii, S. & Shiota, K. 2007. Computerized three-dimensional analysis of the heart and great vessels in normal and holoprosencephalic human embryos. *Anatomical record : advances in integrative anatomy and evolutionary biology,* 290, 259-67.

Yamada, S., Samtani, R. R., Lee, E. S., Lockett, E., Uwabe, C., Shiota, K., Anderson, S. A. & Lo, C. W. 2010. Developmental atlas of the early first trimester human embryo. *Developmental dynamics : an official publication of the American Association of Anatomists,* 239, 1585-95.

Yamada, S., Uwabe, C., Fujii, S. & Shiota, K. 2004. Phenotypic variability in human embryonic holoprosencephaly in the Kyoto Collection. *Birth Defects Res A Clin Mol Teratol,* 70, 495-508.

Yamada, S., Uwabe, C., Nakatsu-Komatsu, T., Minekura, Y., Iwakura, M., Motoki, T., Nishimiya, K., Iiyama, M., Kakusho, K., Minoh, M., Mizuta, S., Matsuda, T., Matsuda, Y., Haishi, T., Kose, K., Fujii, S. & Shiota, K. 2006. Graphic and movie illustrations of human prenatal development and their application to embryological education based on the human embryo specimens in the Kyoto collection. *Developmental dynamics : an official publication of the American Association of Anatomists,* 235, 468-77.

Yoneyama, A., Takeda, T., Tsuchiya, Y., Wu, J., Lwin, T. T., Koizumi, A., Hyodo, K. & Itai, Y. 2004. A phase-contrast X-ray imaging system—with a 60×30 mm field of view—based on a skew-symmetric two-crystal X-ray inteferometer. *Nuclear Instruments and Methods in Physics Research Section A: Accelerators, Spectrometers, Detectors and Associated Equipment,* 523, 217-222.

Yoneyama, A., Yamada, S. & Takeda, T. 2011. Fine Biomedical Imaging Using X-Ray Phase-Sensitive Technique. *In:* Gargiulo, D. G., Mcewan, A. (ed.) *Advanced Biomedical Engineering*. InTech. p107-128.

Congenital Anomalies
THE JAPANESE TERATOLOGY SOCIETY
doi:10.1111/j.1741-4520.2011.00345.x
Congenital Anomalies 2012; **52**, 55–58

SHORT COMMUNICATION

Morphometric analysis of the brain vesicles during the human embryonic period by magnetic resonance microscopic imaging

Takashi Nakashima[1], Ayumi Hirose[1], Shigehito Yamada[2], Chigako Uwabe[2], Katsumi Kose[3], and Tetsuya Takakuwa[1]
[1]Human Health Science and [2]Congenital Anomaly Research Center, Graduate School of Medicine, Kyoto University, Kyoto, and [3]Institute of Applied Physics, University of Tsukuba, Ibaragi, Japan

ABSTRACT **The development of the brain vesicles between Carnegie stages (CS) 17 and 23 was analyzed morphometrically using 177 magnetic resonance image data derived from the Kyoto Collection of Human Embryos. Whole embryonic volume was 106.55 ± 21.08 mm^3 at CS17, exponentially increasing to CS23 when it reached 1357.28 ± 392.20 mm^3. Length of brain vesicles was 29.83 ± 2.52 mm at CS17, increased almost linearly and reached 49.31 ± 6.66 mm at CS23. The rate of increase was approximately 4.2 times higher on the dorsal side than on the ventral side. The increase in the length of the brain vesicles resulted mainly from that of the prosencephalon, and the rate of increase was three times higher on the dorsal side than on the ventral side of the prosencephalon.**

Key Words: brain vesicle, human embryo, magnetic resonance imaging, morphometry, neural tube

INTRODUCTION

Embryonic development is characterized by dynamic and gross changes in the external appearance in accord with internal organogenesis. The Developmental Horizons and Carnegie Stages (CS) (O'Rahilly 1972; O'Rahilly and Müller 1987) are monumental works, both of which are determined by qualitative observation of the external appearance of the human embryo in accord with internal organogenesis. They have been predominantly used as the most reliable indices of human embryonic development. Further, they have been applied to the staging of various vertebrate embryos (Butler and Juurlink 1987).

Additional quantitative data are indispensable for many studies, such as the study of individual differences, symmetry, rate of growth, evaluation of developmental delay due to various causes, and comparisons with other mammalian species. However, quantitative data on the human embryonic period have been limited to measurement from the outside, such as crown–rump length and body weight. Only a few quantitative studies have dealt with the external features of various parts in developing human embryos (Jackson 1909; O'Rahilly and Müller 1984). Recently, Otani et al. (2008) proposed defined measurements of body parts as well as of the whole body, and established a set of approximate standards. These measurements required arduousness and a high degree of skill to minimize errors. Each embryo was set under a dissecting microscope with an attached scale so that the dimension to be measured was parallel to the surface of the scale.

Correspondence: Tetsuya Takakuwa, MD, PhD, Human Health Science, Graduate School of Medicine, Kyoto University, Sakyo-ku Shogoin Kawahara-cyo 53, Kyoto 606-8507, Japan. Email: tez@hs.med.kyoto-u.ac.jp

Received August 19, 2011; revised and accepted October 2, 2011.

Quantitative observation of internal structures has also been difficult because the internal developmental process has been examined mainly using classic histology-based methods with a small number of samples. Recently three-dimensional (3D) imaging techniques have dramatically improved examination methods. With the advent of magnetic resonance (MR) imaging, the imaging of embryos has proven to be highly effectual (Effmann et al. 1988; Smith et al. 1992; Haishi et al. 2001), providing a resolution of 40 μm/pixel or more with long scan times. MR imaging is a non-invasive and non-destructive method that has many possibilities not only for precise morphological observations but also for morphometric evaluations of internal structures.

The human brain is arguably one of the most complicated organs in living systems (O'Rahilly and Müller 2006; Bayer and Altman 2008; Huang et al. 2009). This elaborate structure originates from a simple neural tube, followed by a series of differentiation processes. Morphometric characterization of the brain vesicles at each stage not only aids in understanding this highly ordered developmental process but also provides clues to detecting abnormalities caused by genetic or environmental factors. In this connection, morphometric data of brain vesicles and whole embryo volume using MR data was provided in the present study. Such methods and obtained morphometric data will pave the way for analyzing human embryos.

MATERIALS AND METHODS

Human embryo specimens

Approximately 44 000 human embryos comprising the Kyoto Collection are historical specimens collected and stored at the Congenital Anomaly Research Center of Kyoto University (Nishimura et al. 1968; Nishimura 1975; Shiota 1991; Yamada et al. 2004). In most cases, pregnancy was terminated during the first trimester for socioeconomic reasons under the Maternity Protection Law of Japan. Some of the specimens (~20%) are undamaged, well-preserved embryos. When the aborted materials were brought to the laboratory, the embryos were measured, examined and staged using the criteria of O'Rahilly and Müller (1987). Approximately 1200 well-preserved human embryos diagnosed as externally normal from CS13 to CS23 were selected for MR microscopic imaging. The conditions used to acquire the MR images of the embryos are described elsewhere; Matsuda et al. 2003, 2007; Yamada 2006; Shiota et al. 2007). The present study was approved by the Committee of Medical Ethics of Kyoto University Graduate School of Medicine, Kyoto, Japan (E986).

MR image processing and selection of the datasets

3D MR image datasets for each embryo were initially obtained from 256 × 256 × 512 voxels. Each dataset was first converted into a two-dimensional (2D) stack and saved as an audio video

interleave (.avi) file format using software ImageJ version 1.42q (National Institutes of Health, Bethesda, MD, USA). Sequential 2D images were re-sectioned digitally and 3D images were reconstructed using the software OsiriX version 3.7.1 (Pixmeo SARL, Geneva, Switzerland). Both 2D and 3D images were carefully observed and selected according to the following conditions: (i) no obvious damage or significant anomaly present in the external appearance; (ii) head and neck axes maintained in the original form (i.e. not deformed artificially during fixation and preservation); and (iii) sufficiently high quality of reconstructed 2D images to properly extract the organs and tissues. For the present study, 177 samples distributed between CS17 and 23, consisting of 25 or more samples for each stage, were selected from the 1200 MR image datasets based on the criteria described above.

3D reconstruction of the embryo and morphometry of the brain vesicles

The present study used 3D images reconstructed using the maximum intensity projection (MIP) module in software OsiriX. The projected 3D images gave both external and internal information. The lateral view of the 3D images on the screen were captured using Screenshot Plus version 3.2 (Steven Chaitoff, CA, USA) and measured using the software Photoshop CS4.0 (Adobe Systems Incorporated, CA, USA). Length was measured by pixel on the image on the screen and then converted to millimeters using voxel/pixel and voxel/mm ratios specific for each embryo.

The length of whole neural tube surrounding was measured, and that was divided into the regions of brain vesicles and spinal cord by the level of C1 for the first cervical vertebra (Fig. 1A). The spinal cord region was further subdivided by the line that connects the acromion and trochanter to dissect the region of spinal cord corresponding to the trunk and tail (Fig. 1B).

The brain vesicles after CS18 were divided into the following six regions according to anatomic landmarks (Fig. 1C): ventral region of the prosencephalon (PV) – the length between the olfactory bulb (ob) and the supramammillary recess (sr); dorsal region of the prosencephalon (PD) – the length between the posterior commissure (pc) and ob; ventral region of the mesencephalon (MV) – the length between the supramammillary recess (sr) and the isthmic recess (ir); dorsal region of the mesencephalon (MD) – the length between pc and the isthmic groove (ig); ventral region of the rhombencephalon (RV) – the length between ir and the level of C1; and dorsal region of the rhombencephalon (RD) – the length between ig and the level of C1.

The volume of the embryo was measured using region growing module in OsiriX.

RESULTS AND DISCUSSION

Whole embryonic volume

The whole embryonic volume was 106.55 ± 21.08 mm^3 at CS17, exponentially increasing until CS23 when it reached 1357.28 ± 392.20 mm^3 (Fig. 2A). The present data may be comparable with the estimated volume of embryos in the first trimester ultrasound recently reported: 310 ± 137 mm^3 at seven weeks and 1017 ± 352 mm^3 at eight weeks of gestational age (Rousian et al. 2010), although staging was not applied to that study.

Brain vesicles

Length of the brain vesicles was 29.83 ± 2.52 mm at CS17, increased almost linearly and reached 49.31 ± 6.66 mm at CS23 (Fig. 2B-a). Length of the dorsal side of the brain vesicle was

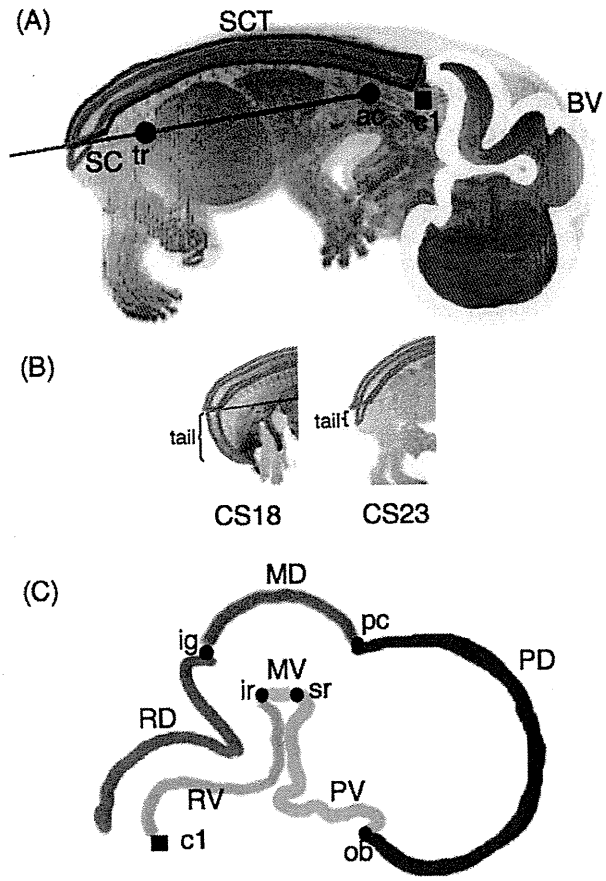

Fig. 1 (A) Lateral view of 3D images reconstructed by maximum intensity projection with drawing showing measurement of brain vesicles. The length of whole neural tube surrounding was measured and divided into the regions of brain vesicles and spinal cord by the level of the first cervical vertebra. The spinal cord was further subdivided by the line that connects the acromion and trochanter to dissect the region of spinal cord corresponding to the trunk and tail. (B) Magnification of spinal cord corresponding to 'tail' region at Carnegie Stage (CS) 18 and CS23. (C) Drawing showing region of the three brain vesicles. Anatomic landmarks for segmentation are indicated: ventral (PV) and dorsal (PD) region of the prosencephalon; ventral (MV) and dorsal (MD) region of the mesencephalon; ventral (RV) and dorsal (RD) region of the rhombencephalon. Ac, acromion; BV, brain vesicles; C1, first cervical vertebra; ig, isthmic groove; ir, isthmic recess; ob, olfactory bulb; pc, posterior commissure; SC, spinal cord; SCT, spinal cord without tail; sr, supramammillary recess; tr, trochanter.

22.85 ± 1.74 mm at CS18, increased linearly and reached 33.38 ± 3.23 mm at CS23 (Fig. 2B-b). While length of the ventral side of the brain vesicle increased only marginally, namely 15.61 ± 1.04 mm at CS18 and 18.11 ± 1.77 mm at CS23, the rate of increase was approximately 4.2 times higher on the dorsal side than on the ventral side.

The dorsal side was analyzed by three primary vesicles: prosencephalon, mesencephalon and rhombencephalon (Fig. 2B-c). Length of the dorsal side of the prosencephalon was 5.65 ± 0.69 mm at CS18, increased linearly and reached 13.75 ± 1.76 mm at CS23. Length of the dorsal side of the mesencephalon was

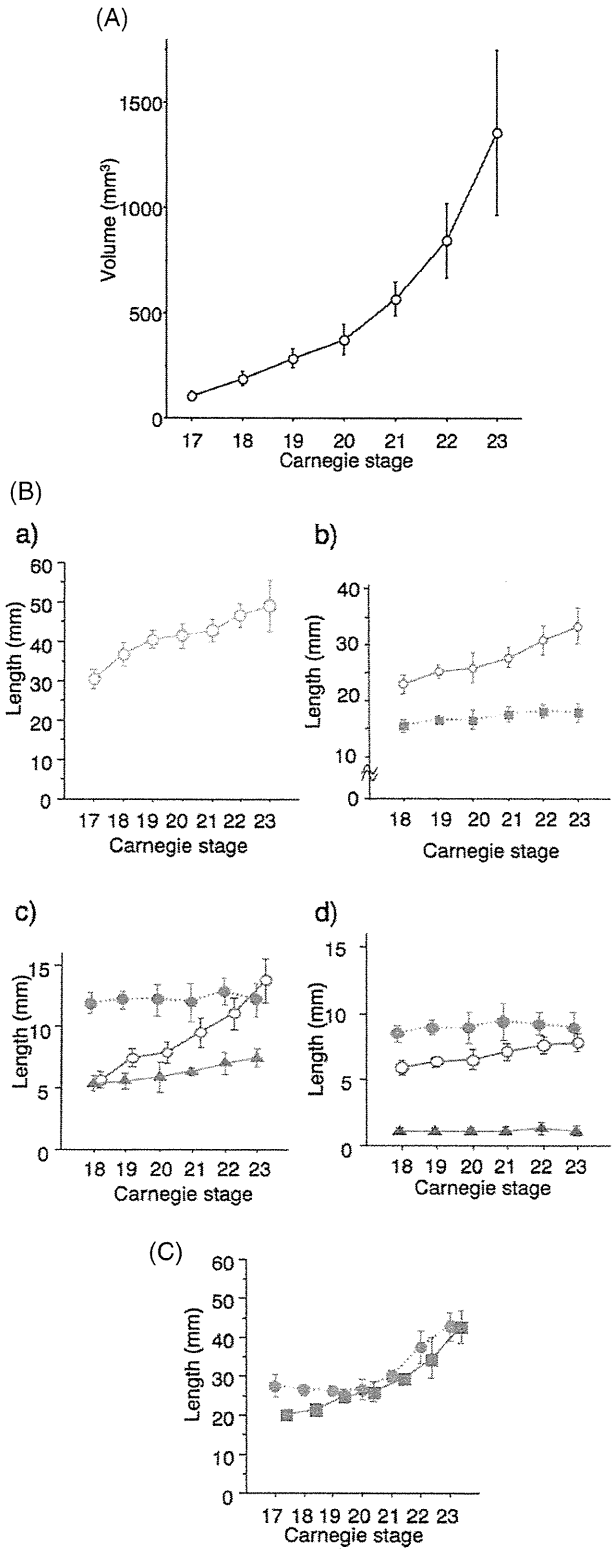

Fig. 2 Morphometry of 3D images from human embryo. (A) Whole embryo volume according to Carnegie stages. (B) Change of length in brain vesicles during development. (a) Change of length in brain vesicles during development. (b) Dorsal (○) and ventral (■) length of brain vesicles during development. (c) Dorsal length of brain vesicles by the regions during development. (○) prosencephalon; (▲) mesencephalon; and (●) rhombencephalon. (d) Ventral length of brain vesicles by the regions during development. (○) prosencephalon; (▲) mesencephalon; and (●) rhombencephalon. (C) Morphometry of spinal cord. Change of length in spinal cord (●) and in spinal cord without tail (■).

5.35 ± 0.62 mm at CS18, increased a little and reached 7.45 ± 0.72 mm at CS23. Length of the dorsal side of the rhombencephalon was almost constant, ranging from 11.85 to 12.86 mm between CS18 and CS23.

The ventral side was also analyzed by the three primary vesicles (Fig. 2B-d). Length of the ventral side of the prosencephalon was 5.66 ± 0.56 mm at CS18, increased linearly and reached 7.88 ± 0.68 mm at CS23. Length of the ventral side of the mesencephalon and the rhombencephalon was almost constant, ranging from 1.22 to 1.43 mm for the former, and from 8.51 to 9.39 for the latter between CS18 and CS23.

The present data revealed that the increase in length of the brain vesicle resulted mainly from that of the prosencephalon, and that the rate of increase was approximately three times higher on the dorsal side than on the ventral side of the prosencephalon.

Spinal cord

Length of the spinal cord was almost constant, ranging from 26.42 to 27.50 mm between CS17 and CS20, then gradually increased and reached 42.82 ± 3.86 mm at CS23 (Fig. 2C). Length of the spinal cord without the tail region (SCT) was 19.88 ± 0.86 mm at CS17, increased gradually and reached 42.59 ± 4.27 mm at CS23.

The difference between spinal cord and SCT, which corresponds to the length of the 'tail region' was 7.62 mm at CS17, and then decreased until CS20, indicating the shortening of the tail region (Fig. 1B). This difference was only between 0.16 and 0.23 mm after CS20.

The present study has demonstrated that analysis using 3D reconstructed images was a useful tool for morphometric evaluations of the internal structures. During morphometric analysis, the projected image was rotated three dimensionally and a lateral image was selected. Then the precise length of the dorsal and ventral lines of the brain vesicles was measured quantitatively, which may reflect the growth of the respective regions. The quantitative data indicate the growth of the respective brain vesicles and spinal cord, as well as dynamic morphogenesis, such as cephalic flexure, cervical flexure and pontine flexure. Morphometric characterization of the brain vesicles at each stage not only aids in understanding this highly ordered developmental process but also provides clues to detecting abnormalities caused by genetic or environmental factors.

ACKNOWLEDGEMENTS

We are deeply indebted to Executive Vice President of Kyoto University, Kohei Shiota, for providing the invaluable MR data. We also acknowledge the contribution of collaborating obstetricians and the previous members of the Congenital Anomaly Research Center, Graduate School of Medicine, Kyoto University. This study was supported by Grant Nos 22591199, 228073, 238058, and 21790180 from Japan Society for the Promotion of Science and BIRD of Japan Science and Technology Agency (JST).

REFERENCES

Bayer SA, Altman J. 2008. The human brain during the early first trimester. London: CRC; Taylor and Francis.

Butler H, Juurlink BHJ. 1987. An atlas for staging mammalian and chick embryos. London: CRC Press.

Effmann EL, Johnson GA, Smith BR, Talbott GA, Cofer G. 1988. Magnetic resonance microscopy of chick embryos in vivo. Teratology 38:59–65.

Haishi T, Uematsu T, Matsuda Y, Kose K. 2001. Development of a 1.0 T MR microscope using a Nd-Fe-B permanent magnet. Magn Reson Imaging 19:875–880.

Huang H, Xue R, Zhang J et al. 2009. Anatomical characterization of human fetal brain development with diffusion tensor magnetic resonance imaging. J Neurosci 29:4263–4273.

Jackson CM. 1909. On the prenatal growth of the human body and the relative growth of the various organs and parts. Am J Anat 9:119–165.

Matsuda Y, Utsuzawa S, Kurimoto K et al. 2003. Super-parallel MR microscope. Magn Reson Med 50:183–189.

Matsuda Y, Utsuzawa S, Kurimoto T et al. 2007. Imaging of a large collection of human embryo using a super-parallel MR microscope. Magn Reson Med Sci 6:139–146.

Nishimura H. 1975. Prenatal versus postnatal malformations based of the Japanese experience on induced abortions in the human being. In: Blandau RJ, editor. Aging gametes. Basel: S. Karger AG. p 349–368.

Nishimura H, Takano K, Tanimura T, Yasuda M. 1968. Normal and abnormal development of human embryos: first report of the analysis of 1213 intact embryos. Teratology 1:281–290.

O'Rahilly R. 1972. Guide to the staging of human embryos. Anat Anz 130S:556–559.

O'Rahilly R, Müller F. 1984. Embryonic length and cerebral landmarks in staged human embryos. Anat Rec 209:265–271.

O'Rahilly R, Müller F. 1987. Developmental stages in human embryos: including a revision of streeter's horizons and a survey of the Carnegie collection. Washington, DC: Carnegie Institution of Washington.

O'Rahilly R, Müller F. 2006. The embryonic human brain: an atlas of developmental stages, 3rd edn. Hoboken: Wiley-Liss.

Otani H, Udagawa J, Lundh T et al. 2008. Morphometric study on the characteristic external features of normal and abnormal human embryos. Congenit Anom (Kyoto) 48:18–28.

Rousian M, Koning AH, van Oppenraaij RH et al. 2010. An innovative virtual reality technique for automated human embryonic volume measurements. Hum Reprod 25:2210–2216.

Shiota K. 1991. Development and intrauterine fate of normal and abnormal human conceptuses. Congenit Anom (Kyoto) 31:67–80.

Shiota K, Yamada S, Nakatsu-Komatsu T et al. 2007. Visualization of human prenatal development by magnetic resonance imaging (MRI). Am J Med Genet A 143:3121–3126.

Smith BR, Effmann EL, Johnson GA. 1992. MR microscopy of chick embryo vasculature. J Magn Reson Imaging 2:237–240.

Yamada S. 2006. Embryonic holoprosencephaly: pathology and phenotypic variability. Congenit Anom (Kyoto) 46:164–171.

Yamada S, Uwabe C, Fujii S, Shiota K. 2004. Phenotypic variability in human embryonic holoprosencephaly in the Kyoto Collection. Birth Defects Res A Clin Mol Teratol 70:495–508.

HEAD & FACE MEDICINE

RESEARCH Open Access

Movement of the external ear in human embryo

Miho Kagurasho[1], Shigehito Yamada[2], Chigako Uwabe[2], Katsumi Kose[3] and Tetsuya Takakuwa[1*]

Abstract

Introduction: External ears, one of the major face components, show an interesting movement during craniofacial morphogenesis in human embryo. The present study was performed to see if movement of the external ears in a human embryo could be explained by differential growth.

Methods: In all, 171 samples between Carnegie stage (CS) 17 and CS 23 were selected from MR image datasets of human embryos obtained from the Kyoto Collection of Human Embryos. The three-dimensional absolute position of 13 representative anatomical landmarks, including external and internal ears, from MRI data was traced to evaluate the movement between the different stages with identical magnification. Two different sets of reference axes were selected for evaluation and comparison of the movements.

Results: When the pituitary gland and the first cervical vertebra were selected as a reference axis, the 13 anatomical landmarks of the face spread out within the same region as the embryo enlarged and changed shape. The external ear did move mainly laterally, but not cranially. The distance between the external and internal ear stayed approximately constant. Three-dimensionally, the external ear located in the caudal ventral parts of the internal ear in CS 17, moved mainly laterally until CS 23. When surface landmarks eyes and mouth were selected as a reference axis, external ears moved from the caudal lateral ventral region to the position between eyes and mouth during development.

Conclusion: The results indicate that movement of all anatomical landmarks, including external and internal ears, can be explained by differential growth. Also, when the external ear is recognized as one of the facial landmarks and having a relative position to other landmarks such as the eyes and mouth, the external ears seem to move cranially.

Keywords: External ear, Internal ear, Three-dimensional kinetics, Human embryo, MR imaging

Introduction

External ears, one of the major face components, show an interesting movement during craniofacial morphogenesis in human embryo. The external ear is evidently recognizable after Carnegie stage (CS) 16, and its movement has been described in most embryology textbooks as well [1-5]. The external ears are contained in the lower neck region at CS 17. With the development of the face structure, they ascend to the side of the head at the level of the eyes [6-10]. Streeter [11] has described the essential and precise external movement. The two auricular areas nearly meet in the mid-ventral region in a 6 mm-embryo; they are gradually moved laterally and dorsally. Streeter suggested that the movement of the external ear might be relative rather than real because the external ear is located at the side of the mouth during the development. In the recent study, Gasser [12] proposed that positional changes of the developing structures could be explained by differential growth (i.e. changes in the size and shape of the embryo and its parts) rather than migration (i.e. structures moving from one region of the embryo to another). Gasser demonstrated the evidence by showing the following three examples: sclerotome formation from the somite, spinal ganglion formation from the neural crest, and thymus, thyroid and parathyroid gland formations from pharyngeal endoderm. He emphasized the use of more centralized and less mobile reference points and comparison of both external and internal structures together in the identical magnification for better understanding of the positional changes of the developing structures.

* Correspondence: tez@hs.med.kyoto-u.ac.jp
[1]Human Health Science, Graduate School of Medicine, Kyoto University, 606-8507, Sakyo-ku Shogoin Kawahara-cyo 53, Kyoto, Japan
Full list of author information is available at the end of the article

The present study was aimed at resolving the question - could such a dynamic movement as external ear also be explained by differential growth? MR imaging data of human embryos from the Kyoto Collection of Human Embryos [13]; http://bird.cac.med.kyoto-u.ac.jp] was used for tracing the 3D absolute position of the anatomical landmarks. The MR data had the advantage of comparing facial structures between different stages with identical magnification. Data revealed that positional changes of external and internal ears that occur during morphogenesis could be explained by differential growth.

Materials and methods

Human embryo specimens

Around 44,000 human embryos (constituting the Kyoto Collection) were historical specimens collected and stored at the Congenital Anomaly Research Center of Kyoto University [14-16]. In most cases, pregnancy was terminated during the first trimester for socioeconomic reasons under the Maternity Protection Law of Japan. Some of the specimens (~20%) were undamaged, well-preserved embryos. When the aborted materials were brought to the laboratory, the embryos were measured, examined, and staged using the criteria of O'Rahilly and Müller [10]. Approximately 1,200 well-preserved human embryos diagnosed as externally normal at CS 13 to CS 23 were selected for MR microscopic imaging. The conditions used to acquire the MR images of the embryos are described elsewhere [17,18].

MR image processing and selection of datasets

3D MR image datasets for each embryo were initially obtained from 256 × 256 × 512 voxels. Each dataset was first converted into a two-dimensional (2D) stack and saved as an audio video interleave (.avi) file format using software ImageJ™ (version 1.42q, National Institutes of Health, Bethesda, MD). Sequential 2D images were resectioned digitally and 3D images were reconstructed using the software OsiriX™ (version 3.7.1, Pixmeo SARL, Geneva, Switzerland). Both 2D and 3D images were carefully observed and selected according to the following conditions: 1) no obvious damage or significant anomaly present in the external appearance; 2) body axes maintained in the original form, i.e. not deformed artificially during fixation and preservation; 3) sufficiently high quality of reconstructed 2D images to properly extract the organs and tissues. For the present study, 171 samples between CS 17 and 23 were selected from all 1,200 MR image datasets based on the criteria described above. The number of cases for each CS was distributed between 18 and 30.

Anatomical landmarks

The 3D coordinate was initially given for 13 selected landmarks by examining the position of the voxel on 2D sequential and 3D images using OsiriX (Figure 1). The selected 13 landmarks were as follows: bilateral auricular hillock on the first cranial arch which becomes tragus later (Ex1), bilateral auricular hillock on the second cranial arch which becomes antitragus later (Ex6) and vestibule (Int) as representative external and internal ear landmarks; stomodeum which becomes a part of mouth (Mo), bilateral nasal pits (Np), bilateral lens vesicles which become a part of eyes (Ey) as external anatomical landmarks, and infundibulum of diencephalons (later pituitary gland) (Pg) and cranial region of the first cervical vertebra (C1) as internal anatomical landmarks.

Evaluation of the position of anatomical landmarks

Two kinds of methods were used to evaluate and analyze the position of the anatomical landmarks in the present study (Figure 2A). Method-1 was used for evaluating the absolute position while Method-2 was for the relative position of each landmark.

Method-1 (Measurement of the absolute position) The 3D absolute position of the anatomical landmarks from MR image data was used to compare the position of each anatomical landmark between the different stages with identical magnification. The line connecting C1 and Pg was defined as reference axis (Z-axis) of 3D orthogonal coordinate for this purpose. Both C1 and Pg are less mobile internal structures close to notocord and detectable during the development [1,19]. Distances between bilateral Ex1s, and collateral Ex1 and Int were calculated and defined as L_{EE} and L_{EI} respectively (Figure 2B). The middle point of the collateral Ex1 and Ex6 were defined as Exm.

Method-2 (Measurement of the relative position) The relative position of the external ears with other landmarks during craniofacial morphogenesis was observed from the frontal position of the face at each stage. For this purpose, the line connecting the middle point of the bilateral Eys and Pg was defined as reference axis (X-axis). The vertical line to the X-axis which contained Mo was defined as Z-axis of 3D orthogonal coordinate. The XY plane defined by this method was almost parallel to the structures at the base of the skull, which divide the area between the neurocranium and viscerocranium [1]. Further, the distance between the middle point of bilateral Eys and Mo was kept constant at one so as to adjust the expansive growth of the face (Figure 2A).

This study was approved by The Committee of Medical Ethics of Kyoto University Graduate School of Medicine, Kyoto, Japan (E986).

Results

Absolute position of internal and external ear and anatomical landmarks

The 3D absolute position of the anatomical landmarks was shown using Method-1. All landmarks moved away

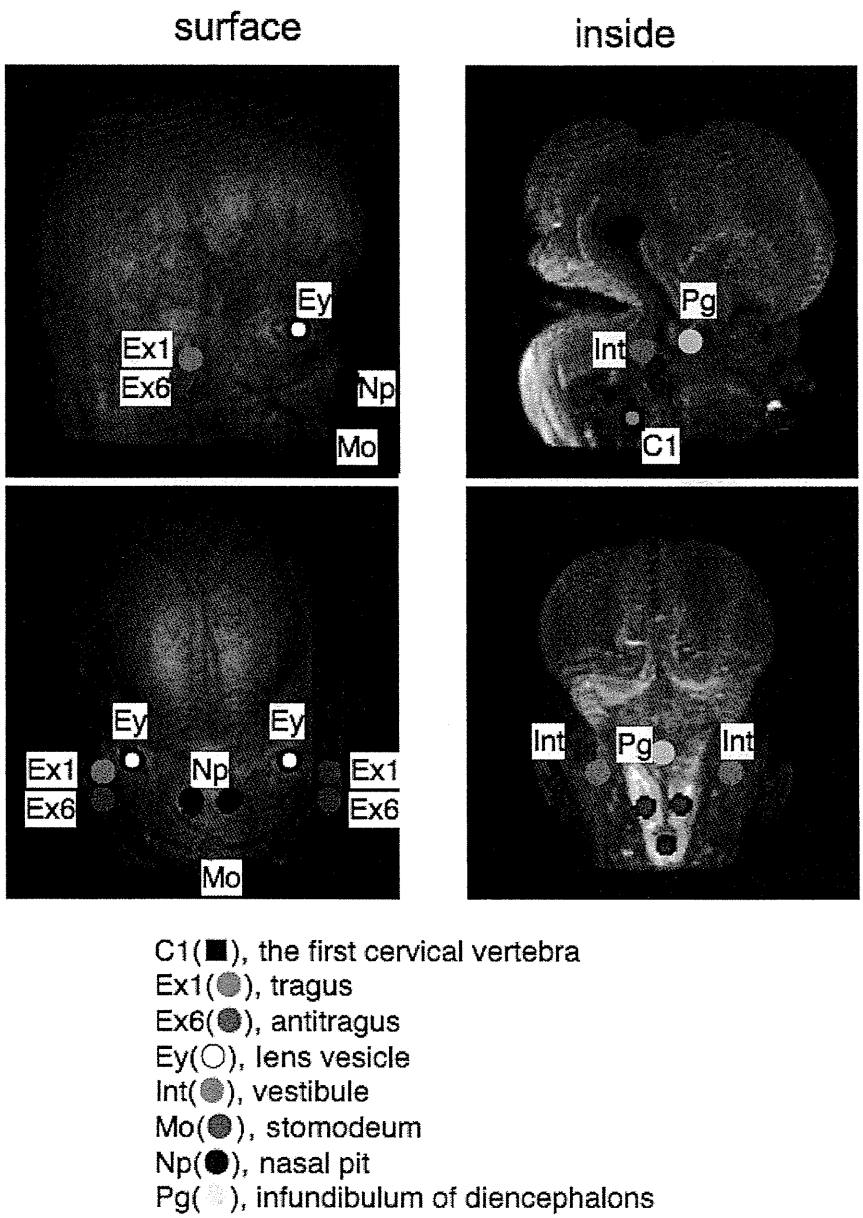

Figure 1 The 13 landmarks selected for present study. Landmarks were expressed on volume rendering 3D images of the head region for surface and maximum intensity projection for inside constructed with software OsiriX.

from the origin (C1) by frontal view (Figure 3A). The line connecting Pg, Ey and Np became longer, which might indicate swelling of the face. Ex1, Ex6 and Int also moved away from the origin (C1) like other landmarks, except that the movement of Int between CS 17 and CS 20 was slow.

By right lateral view, the lines connecting Pg, Ey, Np and Mo, resembling the side view of the swelling face, also became larger as development proceeded (Figure 3B). The movement of Ex1, Ex6 and Int was different from that of the other landmarks. They rotated clockwise for Ex1 and anti-clockwise for Ex6 and Int around CS 17 and CS 21; after that, they moved dorso-cranially.

The position of each landmark in the cranial direction between CS 17 and CS 23 was demonstrated (Figure 3C). All landmarks changed positions smoothly and

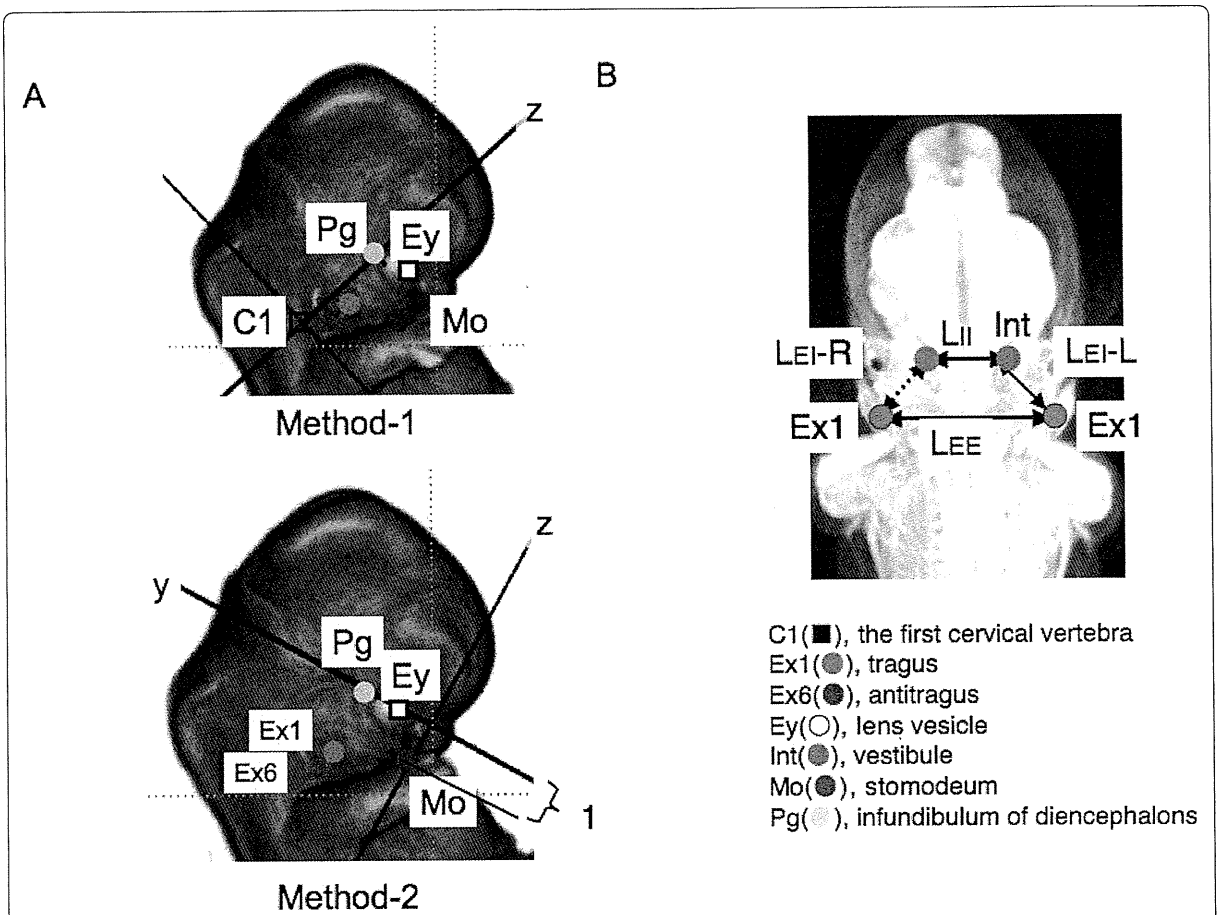

Figure 2 Lateral view showing reference axes, anatomical landmarks and morphometry in present study (A) Reference axes used in Method-1 and Method-2. Reference axes and landmarks were expressed on volume rendering 3D images of the head region constructed with software OsiriX. (B) Anatomical landmarks and morphometry measured in present study. Landmarks were expressed on maximum intensity projection 3D images of the head region constructed with software OsiriX for inside viewing. Distances between bilateral Ex1s, bilateral Ints and collateral Ex1 and Int were defined as L_{EE}, L_{EI}, and L_{EI}, respectively.

gradually during development. As for Int, Ex1, and Ex6, the movement of the position along the cranial/caudal direction was very limited.

Distance and 3D relationship between internal and external ear

L_{EE} and L_{II} increased as CS proceeded (Figure 4). L_{EE} at CS 17 was 2.43+/-0.20 mm (mean +/-SD), and reached 7.38 +/-0.72 mm at CS23. L_{II} at CS 17 was 2.52+/-0.18 mm, and reached 4.63+/-0.41 mm at CS 23. L_{EE} may correspond to the lateral growth of the face, whereas L_{II} corresponds to the lateral thickness of the neural tube. Interestingly, both L_{EI}-L and L_{EI}-R were kept approximately constant, with distribution between 1.42 and 2.01 mm.

Three-dimensionally, the external ear (Exm) located vent-caudal parts of the internal ear in CS 17, and then moved mainly laterally (Figure 5). Exm rotated approximately 49 degrees during CS 17 and CS 23 when Int was the origin (data not shown).

Relative movement of external and internal ear

The relative movement of anatomical landmarks including Ex1, Ex6, and Int was demonstrated using Method-2 (Figure 6). Most landmarks gathered toward the origin as CS proceeded. The relative movement was noticeably larger in Ex1, Ex6, and Int than in Eys, Np, and Pg. Ex1 and Ex6 moved from the caudal lateral ventral region toward the origin. They moved with high speed between CS 17 and 20, and then located and almost stayed between Eys and Mo after CS 21 (Figure 6C). Int migrated from the caudal dorsal lateral region and almost stayed there after CS 21 as well.

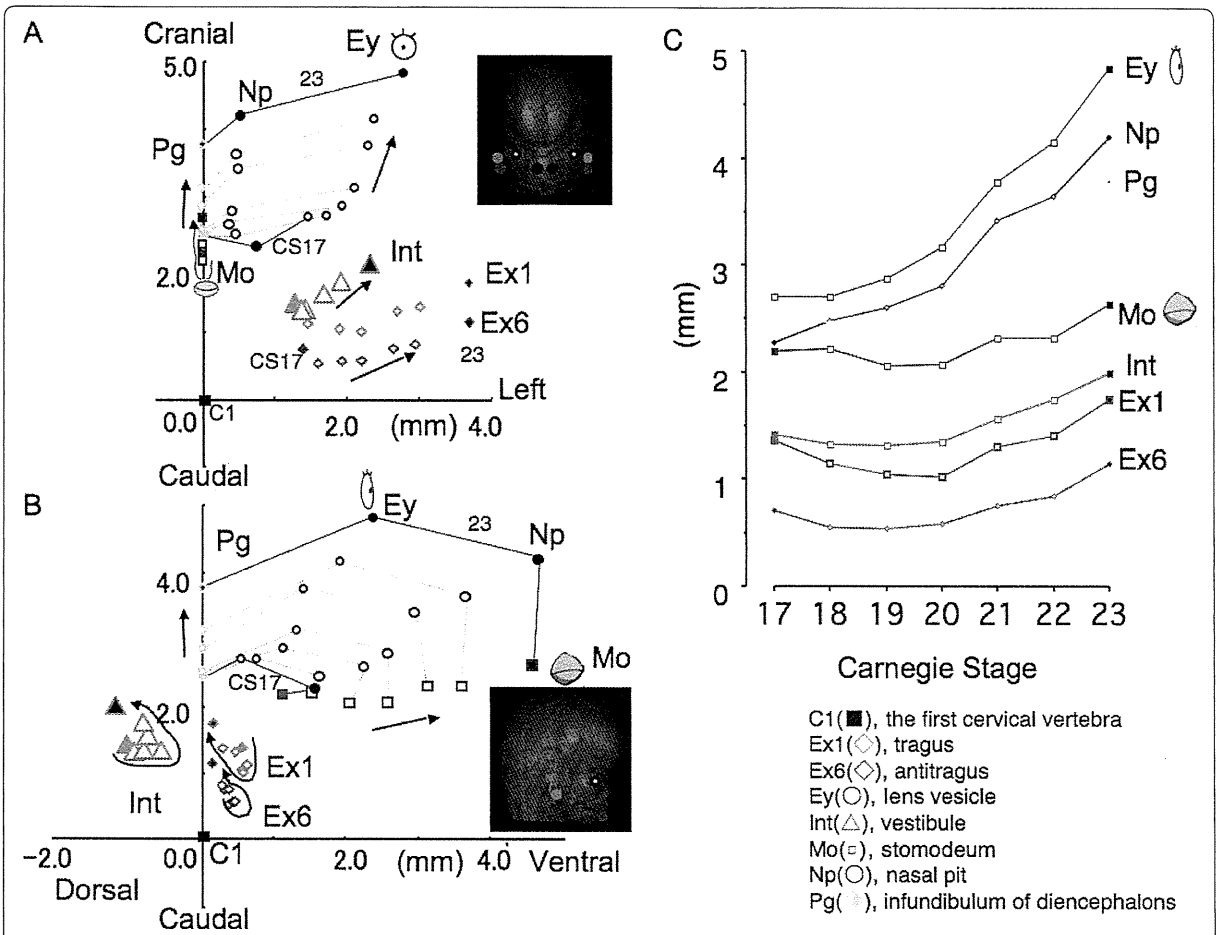

Figure 3 Movement of external and internal ear and anatomical landmarks during development in the orthogonal coordinate defined in Method-1. Frontal view (A) and lateral view (B). The line which connects the pituitary gland and the first cervical vertebra was reference axis (Z-axis) (See also Figure 2). (C). Movement of anatomical landmarks along the reference (Z)-axis.

Discussion

In a recent study, Gasser [12] proposed that some events of mammalian embryogenesis can result from differential growth. Gasser pointed out that dramatic changes occur in size and shape of the embryo and its internal structures but these changes were not considered in past studies that described migratory movements. The present study was performed to reveal whether the movement of human external ears could also be explained as differential growth.

As a principle of physics, all movements occur in relation to a reference point. Thus, it is important to select appropriate references. Gasser [12] claimed that the ideal reference point would be one in the center of the mass, i.e. a centroid. Even though no such consistently occurring point exists in developing embryos, any point that is more centrally located would move less in relation to surrounding structures and therefore would be more suitable. Two methods were used to evaluate the position of the anatomical landmarks in the present study. Method-1 was planned according to Gasser's opinion. The authors selected both C1 and Pg as an ideal reference axis. These were the most central of the embryonic structures located along the notochord. The notochord is an important structure for vertebrate animals, determining the cranial/caudal axis and dividing left and right. It runs along the neural tube and the anterior tip of the notochord reaches an area where the Pg starts to develop [1,19]. C1 body segment is used as one of the reference points in Gasser's study [12]. Another reason for selecting these points was that both were clearly detectable in all stages analyzed.

Movement of 13 anatomical landmarks displayed on the orthogonal coordinate in Method-1 demonstrated that they spread out within the same region as the embryo enlarges and changes shape. The result indicated

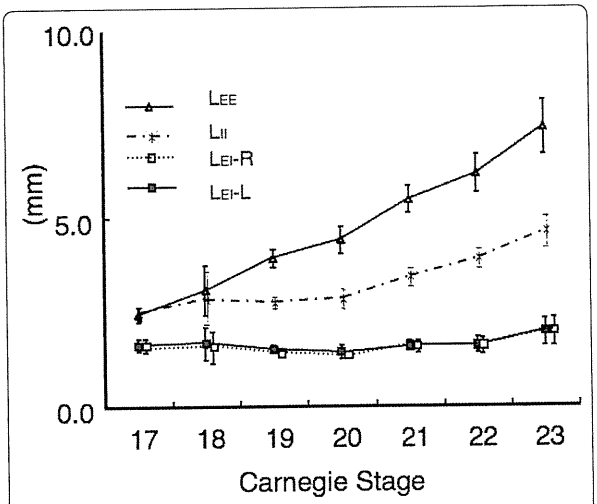

Figure 4 Distance between external and internal ears. Distances between bilateral external ears (L_{EE}), bilateral internal ears (L_{II}), and left internal and external ears (L_{EI}-L) and right internal and external ears (L_{EI} -R) are shown according to CS. (See also Figure 2C.) L_{EE} and L_{II} increase with development, whereas, L_{EI}-L and L_{EI} -R remain approximately constant between CS 17 and CS 23

that the positional changes that occur during the movement of the all anatomical landmarks including external and internal ears could be explained by differential growth.

The external ear did move mainly laterally, but not cranially. In the previous study, Streeter [11] had described that external ears gradually moved laterally and dorsally. As for cranial movement, Streeter suggested that the movement might be relative rather than real because the external ear is located at the side of the mouth during the development. Movement of the external ears along the dorsal/ventral axis was different from that of other anatomic landmarks such as the eyes, nose and mouth. The difference may result from the prominences they are derived from. Face components are formed from five facial primordia which appear early in the fourth week around the Mo [6-9,20,21]. Ey and Np were derived from the nasal prominence located cranial region of the Mo, while Ex1 and Ex6 were from the first and second pharyngeal arches respectively, which were located caudal region of the Mo.

In the present study the movement of the internal ear was limited in all directions. The internal ear develops from the otic placode that appears on either side of the

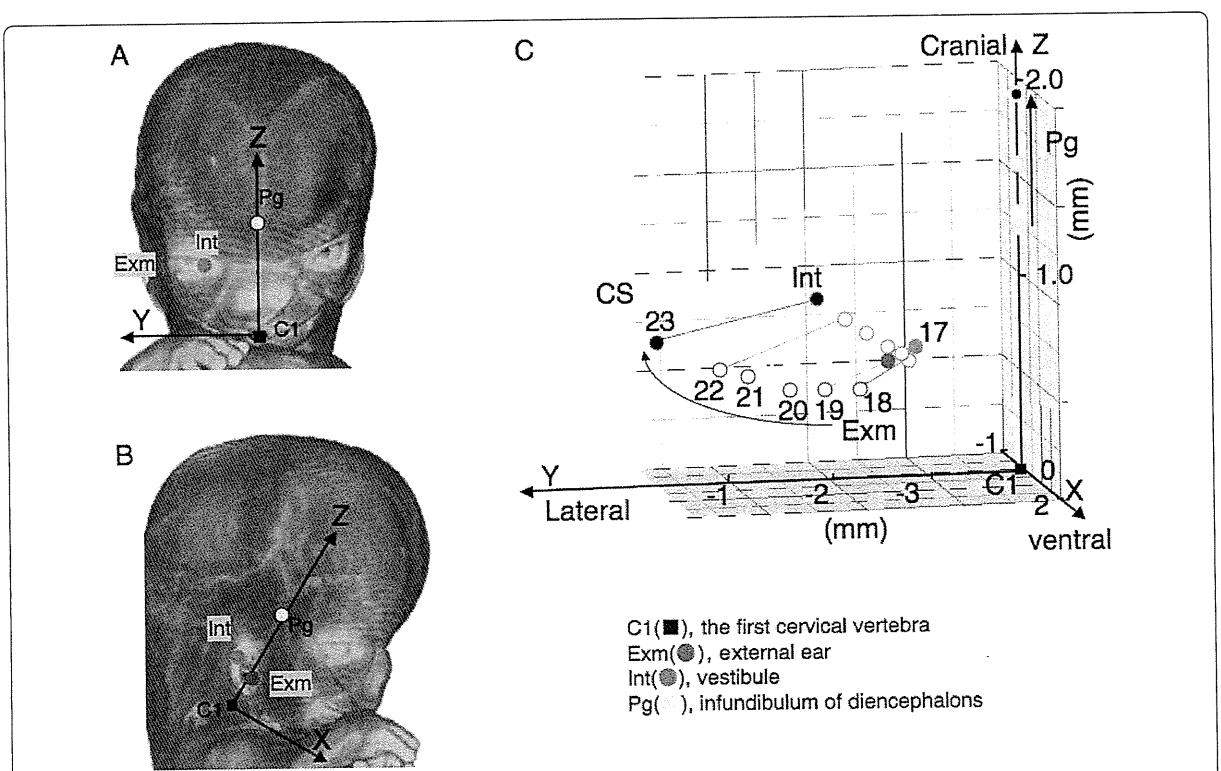

Figure 5 Relationship between right external and internal ears during development. Axes and anatomical landmarks are shown on frontal (A) and lateral (B) views of volume rendering images. (C) Three dimensional graph showing the relationship between right external and internal ears during development.

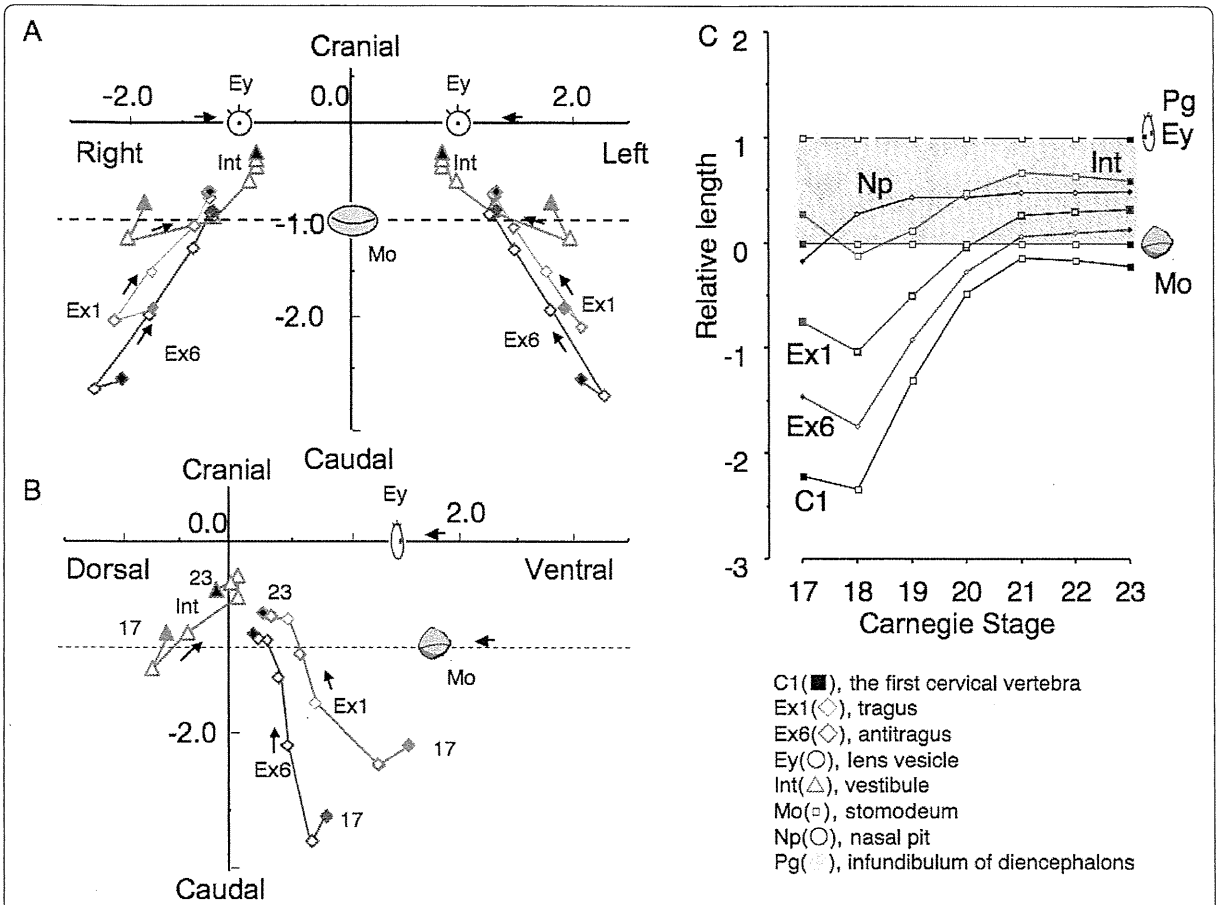

Figure 6 Movement of external and internal ear and anatomical landmarks during development in orthogonal coordinate defined in Method-2. Frontal (A) and left lateral (B) aspects of the face. Line connecting the middle point of the bilateral lens vesicle (Eys) and pituitary gland (Pg) was defined as reference axis (X-axis). The vertical line to the X-axis, which contained Stomodium (Mo) was defined as Z-axis of 3D orthogonal coordinate. The relative position of anatomical landmarks including Ex1, Ex6 and Int is compared with the distance between XY plane and Mo at each CS. (C) Movement of anatomical landmarks along the cranial/caudal (Z)-axis in the orthogonal coordinate in Method-2

neural tube at the level of the future hindbrain or metencephalon [1-4]. Sensory nucleoli of the vestibulocochlear complex are located close to the inner ear. Therefore, it seems hard to move the internal ear from the initial place. The distance between the external and internal ear was almost constant. This was anticipated, considering that all components of the ear relating to the sound-conducting apparatus of the middle and external ears and of the neurosensory structures of the internal ear develop simultaneously throughout development [5].

Surface reference point, i.e. Eys and Mo was adopted in Method-2 for comparison. To observe from the frontal position of the face in all stages, internal structure Pg was also selected. As expected, the movement in the orthogonal coordinate resembled our institutional macro-observation. The present data demonstrated the evident movement of the external ear from the ventral lateral caudal region to the region between the eyes and mouth.

Very different conclusions may be reached about movements of structures by selecting different references in the two methods. The difference may be owing to the following reasons:

1) The magnification of the embryo in all stages was identical in Method-1 while it was adjusted in Method-2. As a consequence, the relative position to the representative landmarks, Eys and Mo may be emphasized in Method-2. Undoubtedly, Eys and Mo are the most important landmarks to recognize the face and these are the landmarks by which the relative position of other landmarks was recognized.

2) There was a gross change of angle between the reference axes used between CS 17 and CS 23 (Figure 7). The change of angle may result from the formation of

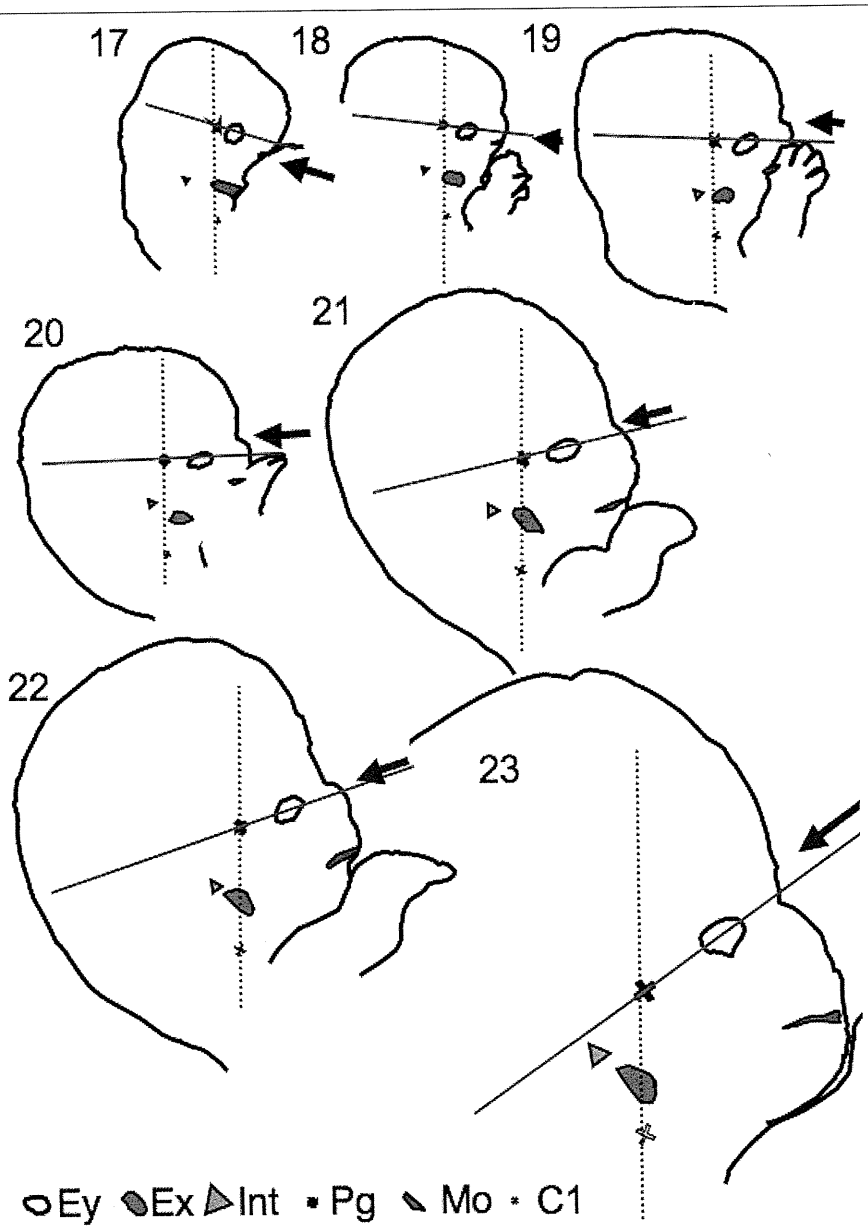

Figure 7 Lateral view of embryos between CS 17 and CS 23 showing craniofacial morphogenesis. The dashed line indicates the reference axis (Z-axis) in Method-1 and the red line indicates the reference axis (X-axis) in Method-2. The arrow indicates the frontal side of the face defined in Method-2. The following anatomical landmarks are drawn: external ear (Ex), internal ear (int), eye (Ey), mouth (Mo), pituitary gland (Pg), and first cervical vertebra (C1). Magnification is identical in all stages. The frontal position defined by Method-2 rotated as stages proceed. Note that both external and internal ears were located at similar positions between Pg and C1 between CS 17 and 23

the mandibular apparatus and the structures at the base of the skull as described in Streeter's study [11]. Pharyngeal arches, especially the first arch, play an important role in the formation of the face [1-5]. In addition to the external ear, many landmarks such as the maxilla, mandible, and a part of middle ear (the incus and malleus) are formed. The development of the mandibular apparatus may move the center of the face in the caudal direction, as well as push the external ear to the lateral side, as both are derived from first pharyngeal arches. Abnormal development of the components of the first pharyngeal arch results in various congenital anomalies of the face including mandible and ears [22]. The development of the structures at the base of the skull and its contents, i.